# Nonlinear onset of calcium wave propagation in cardiac cells

Yohannes Shiferaw

Phys. Rev. E **94**, 032405 — Published 14 September 2016

DOI: 10.1103/PhysRevE.94.032405

# Nonlinear onset of calcium wave propagation in cardiac cells

Yohannes Shiferaw

*Department of Physics & Astronomy, California State University, Northridge,*
*18111 Nordhoff Street, Northridge, CA 91330*

## Abstract

Spontaneous calcium (Ca) waves in cardiac myocytes are known to underlie a wide range of cardiac arrhythmias. However, it is not understood which physiological parameters determine the onset of waves. In this study, we explore the relationship between Ca signaling between ion channels and the nucleation of Ca waves. In particular, we apply a master equation approach to analyze the stochastic interaction between neighboring clusters of Ryanodine Receptor (RyR) channels. Using this analysis, we show that signaling between clusters can be described as a barrier hopping processes with exponential sensitivity to system parameters. A consequence of this feature is that the probability that Ca release at a cluster induces release at a neighboring cluster exhibits a sigmoid dependence on the Ca content in the cell. This nonlinearity originates from the regulation of RyR opening due to more than one Ca ion binding site, in conjunction with Ca mediated cooperativity between RyR channels in clusters. We apply a spatially distributed stochastic model of Ca cycling to analyze the physiological consequences of this nonlinearity, and show that it explains the sharp onset of Ca wave nucleation in cardiac cells. Furthermore, we show that this sharp onset can serve as a mechanism for Ca alternans under physiologically relevant conditions. Thus, our findings identify the nonlinear features of Ca signaling which potentially underlie the onset of Ca waves and Ca alternans in cardiac cells.

***Keywords:*** Calcium waves, calcium signaling, cardiac myocytes.

## I. Introduction

Calcium (Ca) plays an important role in biological cells since it is involved in a wide range of signal transduction pathways [1-4]. In most cells, this is accomplished by a tight spatial and temporal control of the Ca concentration via Ca channels, which transport Ca between intracellular compartments. In the heart, Ca cycles between intracellular stores and this cycling process controls the coupling between membrane voltage and tissue contraction. A crucial signaling molecule involved in Ca cycling is the Ryanodine Receptor (RyR) which controls the flow of Ca from the sarcoplasmic reticulum (SR), which is the main intracellular Ca store. These channels are Ca sensitive and can transition between different conformational states in a Ca dependent manner. Thus, small Ca concentration changes in the vicinity of RyR channels can be amplified by inducing channel openings, which further stimulates the additional flow of Ca. In a cardiac cell, this autocatalytic release process occurs within localized regions surrounding an RyR cluster, and the local increase of Ca concentration is called a Ca spark. This signaling mechanism is referred to as Ca-induced-Ca-release (CICR), and it is used in the cell to mediate important signaling pathways in response to spatially localized Ca concentration changes [3,4]. This amplification mechanism is an important component of the Ca signaling apparatus, which is used in a wide variety of intracellular processes.

RyR clusters are spatially distributed within the three dimensional volume of a cardiac cell. Thus, when a Ca spark occurs at an RyR cluster then Ca can diffuse and elevate the concentration in the vicinity of nearby clusters[4,5]. If this elevation of Ca is large enough then the local Ca release can ignite nearby clusters and propagate in a wave like manner [5-8]. These Ca waves are important since they can lead to triggered activity which can cause cardiac arrhythmias [6,9-11]. A key feature of Ca waves is that their formation is highly sensitive to the Ca concentration in the sarcoplasmic reticulum (SR) [12-16]. Effectively, at low SR Ca concentration, spontaneous Ca sparks occur, but they rarely transition to Ca waves. However, as the SR load is increased, Ca waves begin to form and propagate across the full extent of the cardiac cell. During wave propagation, a substantial amount of Ca can be released in the cell, which can stimulate enough sodium-calcium exchanger to induce a membrane depolarization[17]. Thus, the presence of waves will disrupt the tight coupling between membrane voltage and subcellular Ca release[18]. Under pacing conditions several experimental studies [19,20] demonstrated that Ca waves can also induce Ca alternans, which is a beat-to-beat alternation in the amount of Ca released into the cell. Fluorescence imaging under these conditions demonstrated that waves propagate only on alternate beats, indicating that wave propagation played a key role in the instability to alternans. Using a computational model Tao et al. [21] showed that indeed Ca alternans can be caused by wave propagation which occurred at alternate beats. In a later study Li et al [22] showed that spatial heterogeneity of the Ca signaling system made atrial cells more prone to Ca waves, which led to a steep SR load dependence of release which caused alternans. Also, Nivala et al. [23] showed that the nonlinear regulation of Ca waves due to SR load can drive alternans under conditions of heart failure, where the tight coupling between L-type Ca channels (LCC) and RyR channels is disrupted. These

findings indicate that the onset of Ca waves disrupt the rhythmic response of a cell, and likely plays a key role in various cardiac arrhythmias.

In this paper, we apply theoretical and numerical approaches to determine the factors that govern the onset of Ca waves in cardiac cells. In particular, we analyze how clusters of RyRs interact and compute the probability that a Ca spark at a cluster will induce a neighboring cluster to fire. Our main finding is that this probability distribution function exhibits a sigmoid dependence on system parameters such as the SR load. We show further that this sharp nonlinearity provides a quantitative estimate for the onset Ca wave propagation in a cardiac cell. Our analysis demonstrates that the underlying mechanism for this nonlinearity is due to two essential factors: (i) RyR channels open in a Ca dependent manner regulated by more than one Ca binding site. (ii) RyR channels are arranged in clusters so that Ca release at one receptor induces all the channels to fire. Both of these factors lead to a nonlinear sigmoid dependence of the firing probability on SR load. Our analysis reveals that this nonlinearity is due to a barrier hopping process that is exponentially sensitive to system parameters such as the SR load. Using a detailed stochastic model of Ca cycling we demonstrate that the onset of Ca waves has a sharp sigmoid dependence on the SR load. We show that this sigmoid dependence is due to the nonlinear signaling between neighboring RyR clusters, and present an analytic approximation for the threshold SR concentration. Finally, we show that nonlinear signaling between RyR clusters offers a mechanism for the formation of Ca alternans under certain physiological conditions. This analysis provides a quantitative mechanism linking stochastic dynamics at the ion channel level, and dynamical instabilities at the scale of the whole cell.

## II. Stochastic dynamics of RyR clusters in cardiac myocytes

### A. Computational cell model

To model the spatiotemporal distribution of Ca in ventricular myocytes we have implemented an established mathematical model due to Restrepo et al. [24,25] (Restrepo model). In this model, the myocyte is represented as a collection of subcellular compartments that are distributed in a three dimensional (3D) representation of the cell interior (Figure 1A–C). To model the spatial distribution we denote the Ca concentration in compartment $x$ as $c_x^n$ (Figure 1B), where the superscript $n$ indicates the location of that compartment in a 3D grid representation of the cell interior. The subcellular compartments in the model are: (1) The dyadic junction, with concentration $c_p^n$, where a few LCCs on the cell membrane are in close proximity to a cluster of $\sim 100$ RyR channels attached to the junctional SR (JSR); (2) The submembrane space, with concentration $c_s^n$, which represents a volume in the vicinity of the sarcolemma, which regulates membrane bound ion currents such as the NaCa exchanger and LCC; (3) The bulk myoplasm, with concentration $c_i^n$, which characterizes the volume of space into which Ca diffuses before being pumped back into the SR via SERCA (Sarcoplasmic Reticulum Calcium ATPase) uptake channels;

(4) The junctional SR, with concentration $c_{jsr}^n$, that is the portion of the SR network that is positioned close to the cell membrane; (5) The network SR (NSR), with concentration $c_{nsr}^n$, which represents the bulk SR network that is spatially distributed in the cell. In this study, our cardiac cell model will consist of 60 planes representing Z-planes, where each plane contains an array of $20 \times 20$ regularly spaced compartments (Figure 1C). Ca diffusion in the cell interior is modelled by allowing a diffusive flux between nearest neighbor compartments of the submembrane, the bulk myoplasm, and the SR network. This diffusive flux between nearest neighbors $i$ and $j$ has the form $J_d^{ij} = \Delta c_{ij}/\tau_{ij}$, where $\Delta c_{ij}$ is the concentration difference between the compartments, and $\tau_{ij}$ is the diffusion time constant. In this study we have modified several parameters in the original Restrepo model. In particular we scaled down diffusive time constants between nearest neighbor compartments by a factor of two to promote robust wave propagation at an SR load of roughly $1200\mu M$. The model parameters used in this study are summarized in Table 1, and all parameters not shown are the same as in the original Restrepo model [25]. Finally, we note that the time evolution of RyR and LCC channels are simulated using established Markov state models [11], where the stochastic evolution of the channels is computed according to the reaction rates linking the Markov states.

### B. Master equation approach to modeling Ca signaling between RyR clusters

In this section we develop an analytic approach to explore the conditions for wave propagation in the Restrepo cell model. As a starting point we will first compute the probability, denoted as $p_{ij}$, that a spark at the $i^{th}$ RyR cluster induces a Ca spark at a neighboring cluster $j$. To determine this probability we first simulate the concentration changes due to diffusive fluxes from nearest neighbors on the same Z-plane. In Figure 2A, we plot the dyadic junction Ca concentration at site $i$ when a Ca spark is induced at that junction. In this simulation the initial SR load is fixed at $1000\mu M$ and the concentration during a spark rises to a peak of $\sim 300\mu M$ for a time duration $\tau_s \sim 15ms$. In Figure 2B, we plot the Ca concentration at a nearest neighbor site $j$ on the same Z-plane. Here, we set the RyR conductance in this site to zero in order to measure the rise in local Ca concentration due only to the diffusive flux from the neighboring site $i$. In this case, after a short delay the local Ca concentration rises to roughly $\sim 2.5\mu M$ for a duration similar to the spark lifetime $\sim 15ms$. To compute the probability that this rise in local Ca concentration induces a Ca spark at site $j$, we will approximate the concentration change as a step function of the form

$$c_p(t) = \begin{cases} c_a & 0 < t < \tau_s \\ c_o & t < 0 \ \ and \ \ t > \tau_s \end{cases} \quad (1)$$

where $c_a \sim 2.5\mu M$, $c_o \sim 0.2\mu M$ is the background concentration, and where $\tau_s \sim 15ms$. We note that $c_a$ is dependent on a variety of factors such as the diffusivity of Ca, the distribution of intracellular buffers, and the JSR load. To proceed we note that Ca diffusion within the dyadic junction is in the range $D \sim 100 - 500\ (\mu m)^2/s$ [24,26], so that the diffusion time across a junction is $\sim 0.1 - 0.4\ ms$, which is much faster than the typical RyR

channel transition times. Thus, we can make the rapid diffusion approximation and assume that Ca is spatially uniform within the junction. The local concentration is then $c_p(t) \approx c(t) + gn$ , where $c(t)$ is the concentration due to diffusive fluxes into the junction, $n$ is the number of RyR channels open, and $g$ is the rise in local concentration due to an open RyR channel. This quantity can be approximated as $g \simeq J_r/(2\pi Dh\theta F)$ where $J_r$ is the Ca flux due to an open RyR channel in units of $pA$, $F$ is Faraday's constant, $\theta = 2$ is the charge of the Ca ion, and where $h$ is the height of the dyadic space i.e. the spacing between LCC and RyR channels. Here, we also note that the RyR flux has the form $J_r = g_r(c_{jsr} - c_i) \approx g_r c_{jsr}$, where $g_r$ is the channel conductance, and $c_{jsr}$ is the JSR concentration, which is much larger than the diastolic Ca concentration before the firing of a spark ($c_{jsr} \gg c_i$). These simplifications give the approximate relation $g \simeq \alpha c_{jsr}$ with $\alpha = g_r/(2\pi Dh\theta F)$.

The RyR channel in the Restrepo model is described using a 4-state scheme that accounts for Calsequestrin (CSQN) binding to luminal sites of the RyR [24]. In this study we focus only on activation of an RyR cluster where all the channels are initially in the unbound closed state, and which transition to the unbound open state during a Ca spark. Thus, for this purpose it is sufficient simplify the Markovian model to a two state scheme

$$C \underset{k_-}{\overset{k_+ c_p^\gamma}{\rightleftharpoons}} O \ , \tag{2}$$

where the exponent $\gamma \geq 2$ models the cooperativity of multiple Ca ions binding to the RyR channel, and where the rate constants are the same as the closed to open transition of the CSQN-unbound state of the Restrepo model. Here, we stress that our simplified approach is sufficient only to describes the activation of Ca sparks in clusters, and it does not describe slower processes that depend on RyR channel inactivation and binding to Calsequestrin. The effect of these features will be accounted for in the full stochastic model. Given these assumptions the stochastic dynamics of the cluster is then governed by $P(n,t)$ which is the probability that $n$ of $N$ RyR channels in the cluster are open at time $t$. This quantity obeys a Master equation:

$$\frac{dP(n,t)}{dt} = w_+(n-1)P(n-1,t) + w_-(n+1)P(n+1,t) - \big(w_+(n) + w_-(n)\big)P(n,t), \tag{3}$$

where $w_+(n) = k_+(N-n)\big(c_p + g\,n\big)^\gamma$ and $w_-(n) = k_- n$. Thus, the dynamics is described by a birth-death process with a forward rate that is a nonlinear function of the local Ca concentration.

To proceed we follow our previous work [27], which is based on Hinch et al. [28], and consider the large $N$ limit where the birth-death process can be mapped to the continuum. Then, if we define the fraction of channels in the open state as $x = n/N$, detailed balance between states of the cluster gives an equilibrium distribution

$$p_e(x) \propto \exp\big(-N\Phi(x)\big), \tag{4}$$

where $\Phi(x)$ is the effective potential given by

$$\Phi(x) = -\int_0^x \ln\big(\rho(x')\big)\, dx', \tag{5}$$

and where

$$\rho(x) = \frac{w_+(Nx)}{w_-(Nx)} = \frac{\eta(1-x)(s+Nx)^\gamma}{x}, \tag{6}$$

with dimensionless parameters

$$s = \frac{c_p}{g} \quad , \quad \eta = \frac{k_+ g^\gamma}{k_-} \ . \tag{7}$$

In this picture, $\eta$ is a variable that gives a measure of the cluster excitability, and $s$ measures the interaction between two clusters via the local Ca concentration $c_p$. These two dimensionless quantities characterize the stochastic dynamics of an RyR cluster in which the local concentration has the time dependence given by $c_p(t)$.

*Model parameters.* In order to compute the effective potential, we will determine the parameters $s$ and $\eta$ directly from numerical simulations of the Restrepo cell model. Firstly, we note that the rise in local concentration due to a neighboring spark $c_a$ is proportional to the JSR load. Therefore, we will model the local concentration using a simple linear relation $c_a = \beta c_{jsr}$, where $\beta$ is a constant that characterizes the cluster-to-cluster interaction. Using Figure 2B we estimate that $\beta = 2.5/1000$, since the local concentration rises to $c_p \approx 2.5\mu M$ at a JSR load of $c_{jsr} = 1000\mu M$. To estimate the parameter $g$ we note that $c_p \approx g \cdot n$, so that $g$ can be extracted directly by measuring the local rise in Ca concentration due to the opening of RyR channels in the cluster. Using this approach we estimate that $g \sim 5\mu M$ when the JSR load is $c_{jsr} = 1000\mu M$, which gives $g = \alpha c_{jsr}$ with $\alpha = 5/1000$. Using these estimates we find that when a neighboring spark occurs then $s = s_{on}$ where $s_{on} = \beta/\alpha =$

0.5. Now, when all neighboring units are inactive then $s = s_{off}$ with $s_{off} = 0.2/5 = 0.04$. Hereafter, we will refer to each case as "spark on" and "spark off" respectively. To compute the effective potential we use model parameters taken from the Restrepo model along with the estimates described above (Table 2). In Figure 3A, we plot the effective potential $\Phi(x)$ for small $x$ for the spark off (black line) and spark on case (red line). In the spark off case the effective potential has a stable stationary point at $x_o \sim 0$ which represents the fully shut cluster, and an unstable stationary point at $x_1 \approx 0.03$. For $x > x_1$ the effective potential decreases and reaches a global minimum at $x_2 \sim 1$ (not shown) which represents the fully open cluster. Here, we focus on the small $x$ regime since signaling between clusters is dictated by the changes in the effective potential in this region. In the spark on case the bistable potential tilts and the barrier separating the two stable stationary states is reduced (red line). To determine the stationary points, we note that they satisfy $d\Phi/dx = 0$ which requires that $\rho(x) = 1$. The stationary points are then solutions to the algebraic condition

$$\eta(1 - x)(s + Nx)^{\gamma} - x = 0. \tag{8}$$

In Figure 3B we show the stationary points $x_o$ and $x_1$ as a function of the parameter $s$. Here, we find that as $s$ is increased the stationary points merge and the system becomes monostable with only one global minimum at ($x_2 \sim 1$), which corresonds to the fully open cluster.

### C. Stochastic dynamics of spark activation.

The dynamics of the effective potential allows us to characterize the dynamics of spark activation due to a rise in the local Ca concentration. We first note that for $t < 0$, the effective potential landscape will have the "spark off" shape (Figure 3A, solid black curve) and the system will reside at the stable stationary point at $x_o$, which corresponds to the closed cluster. Once the local concentration rises to $c_a$ then the landscape will shift to the "spark on" shape (red dashed curve). Note that this tilted effective potential has new stationary points that we will denote as $x_o'$ and $x_1'$. Finally, when the diffusive fluxes are turned off for $t > \tau_s$ the landscape returns to the "spark off" shape. Hence, the condition for a spark to be triggered is that the cluster, starting at $x_o$, should cross the barrier peak at $x_1$, within the spark lifetime $\tau_s$. If it does not cross in this time then the system will then roll back to the stationary point at $x_o \sim 0$, and the transition to the open cluster state will not occur i.e. a spark will not fire at that cluster. Here, we note that the crossing dynamics is dictated by the tilted landscape where $s = s_{on}$, while the crossing points are determined by the untilted case with $s = s_{off}$. To determine the probability of triggering a Ca spark we will first consider the limit where $s_{on}$ is small, so that the effective potential in the "spark on" state is still bistable (Figure 3A, dashed red curve). In this case the potential is tilted slightly and spark activation can be viewed as a barrier hopping process where the peak needs to be surmounted. In this limit, the probability that the system crosses $x_1$ in a time $t$ will have an exponential distribution

$$P(t) = \frac{1}{T} \exp\left(-\frac{t}{T}\right) , \tag{9}$$

where $T$ is the mean first passage time (MFPT) for $x$ to make the transition from $x_o$ to $x_1$. This exponential distribution arises from the fact that in this limit the barrier crossing time is still long compared to the time scale of RyR channel fluctuations, so that the crossing rate is approximately constant. The transmission probability is then just the probability of firing in time $\tau_s$, which gives

$$p_{ij} = 1 - \exp\left(-\frac{\tau_s}{T}\right) . \tag{10}$$

Thus, in this limit, the transmission probability is dictated by the ratio of the average spark life time $\tau_s$ and the MFPT for the cluster to undergo a stochastic transition from $x_o$ to $x_1$. Note that for a large tilt, in which the effective potential is monostable, then the exponential distribution above will not hold. In this scenario, we will resort to direct numerical simulations to compute the transmission probability $p_{ij}$.

To compute the mean first passage time $T$ we note that for the cluster to transition from $x_o$ to $x_1$ it is necessary for the system to surmount the barrier height of the tilted effective potential. The escape rate for this to occur is dictated by the stationary points of the tilted effective potential. This is because to leading order the system will spend most of the time near the local minimum at $x_o'$, and if it surrpounts the barrier at $x_1'$, then it is very likely going to cross $x_1$ [29,30] since $x_1 > x_1'$. Following our previous work [14], based on Doering et al. [16], we note that the MFPT has the leading order behavior

$$T \sim \exp(N\Delta\Phi) , \tag{11}$$

where $\Delta\Phi = \Phi(x_1') - \Phi(x_o')$ is the barrier height, and where $x_o'$ and $x_1'$ are the stationary points of the tilted effective potential. In Figure 4A we plot $N\Delta\Phi$ vs the JSR load ($c_{jsr}$) in the "spark on" case where $s = 0.5$. Our results show that there is a critical JSR load, $c_{jsr}^* \approx 1150\mu M$, where $\Delta\Phi\left(c_{jsr}^*\right) = 0$, in which the barrier height is zero. For $c_{jsr} < c_{jsr}^*$ the barrier height increases with decreasing SR load which leads to an exponential increase in the MFPT. To confirm these predictions, we have applied the Gillespie algorithm [17] to compute the exact waiting time statistics of an isolated cluster of $N = 100$ RyR channels obeying the simple reaction scheme given by Eq. (2). In Figure 4B, we plot $T$ vs the JSR load showing the exponential increase in waiting time as the JSR load is decreased. In order to confirm Eq. (10) we have also computed the sparking probability $p_{ij}$. To compute

$p_{ij}$ numerically we hold $s = 0.5$ for a duration $\tau_s = 15ms$, after which $s = 0.04$. We then compute the fraction of independent simulation runs in which the RyR cluster has fired within $50ms$. In these simulations we designate a cluster to have fired when the number of open RyR channels reaches $n = N/2$. In Figure 4C (red dashed curve) we plot $p_{ij}$ computed numerically, along with the prediction of Eq. (10) (black solid line), showing good quantitative agreement. These results indicate that $p_{ij}$ has a sigmoid dependence on the JSR load which is due to the exponential dependence of the MFPT.

### D. The nonlinear properties of stochastic signaling between RyR clusters

Our results indicate that stochastic signaling between clusters will exhibit a strong nonlinear dependence on system parameters. In this section, we will analyze the parameters that control the onset of this nonlinearity. As a starting point, we evaluate the dependence of the barrier height $\Delta\Phi$ on system parameters such as the JSR load. Also, for simplicity we will consider the case $\gamma = 2$, which is the exponent used in the Restrepo model, and which allows for an analytic computation of the stationary points. In this case we can solve for the approximate stationary points and evaluate $\Delta\Phi$. For the parameters considered here we have that $sN\eta < 1$, so that to leading order we have

$$N\Delta\Phi \approx \frac{1}{N\eta} - 2s(1 - \log(N\eta s)) \quad . \tag{12}$$

Within this approximation we can solve for the onset of the exponential nonlinearity by finding the critical SR load $c_{jsr}^*$ such that $\Delta\Phi(c_{jsr}^*) = 0$. Solving for the critical JSR load yields

$$c_{jsr}^* \approx \sqrt{\frac{k_-}{k_+}\frac{q}{N\alpha\beta}} \ , \tag{13}$$

where $q \approx 0.19$ is the solution to the algebraic equation $0 = 1 - 2x(1 - \log(x))$. For the parameters given in Table 2 this gives an estimate for the onset of exponential dependence as $c_{jsr}^* \approx 1000\mu M$. Eq. (10) suggests that the onset of the exponential dependence of the MFPT should be well approximated by the threshold of the sigmoid dependence of $p_{ij}$. In Figure 4D we plot our analytic estimate (Eq. 13) for a range of cluster sizes $N$, and compare to the threshold concentration $c_{th}$ such that $p_{ij}(c_{th}) = 1/2$, where $p_{ij}$ is computed from the exact stochastic simulation. Indeed we find that Eq. (13) gives a good quantitative estimate of the threshold of the transmission probability $p_{ij}$.

In summary, our results indicate that the probability that a Ca spark activates a nearby cluster can be mapped to a barrier hopping process. This hopping process is governed by an effective potential that is determined by the

nonlinear dependence of the RyR channel opening rate on the local Ca concentration. Thus, signaling between clusters will be highly nonlinear, since the transmission probability is dependent on the mean first passage time, which itself is exponentially sensitive to parameters that determine the barrier height. In the following section, we argue that this exponential sensitivity provides a precise criterion for the onset of Ca waves in a computational cell model, and is the underlying nonlinearity that drives alternans under certain physiological conditions.

### III. Wave propagation onset in the 3D stochastic cell model

In this section, we apply the Restrepo cell model to determine the relationship between the transmission probability $p_{ij}$ and the onset of Ca wave propagation. In this model Ca waves occur at elevated SR loads where spontaneous Ca sparks can nucleate a Ca wave in the 3D array of CRUs. In Figure 5A, we show the spatial distribution of Ca in a 2D cross section of a cell with $60 \times 20 \times 20$ CRUs. In this example, we see that Ca waves originate from two nucleation sites and proceed to activate all CRUs in the cell. To characterize the timing of these waves we measured the average diastolic Ca, defined as $c_i(t) = (1/M)\sum_{n=1}^{M} c_i^n(t)$ where $M$ is the total number of CRUs in the cell. This average concentration is roughly $c_i \sim 0.2\mu M$, in the absence of Ca waves, and then rises to a maximum concentration in the range $\sim 1-3\ \mu M$ when a Ca wave occurs in the cell. Thus, the mean waiting time for a Ca wave to occur can be estimated by measuring the time $t_W$ when an intermediate concentration, in this case $c_i(t_W) = 0.7\mu M$, is crossed for the first time. Using this approach we have computed the average waiting time to a wave, denoted as $T_w = \langle t_w \rangle$, by averaging over 100 independent simulations at a fixed initial JSR load concentration $c_{jsr}$. In these simulations the action potential (AP) is fixed at the resting potential of $V = -85mV$. At this voltage the LCC channels are shut and Ca wave nucleation is due only to fluctuations of RyR channels. In Figure 5B, we plot $T_w$ vs $c_{jsr}$ showing that the MFPT to a Ca wave exhibits a strong nonlinear dependence on JSR load. In effect, as the JSR load decreases below the concentration $c_{jsr} \sim 1100\mu M$ the MFPT increases exponentially. In fact, for concentrations below $c_{jsr} \sim 1000\mu M$ Ca waves essentially do not occur within our total simulation time of $3500ms$. In order to present these results within a more physiological setting we have computed the probability that a Ca wave occurs within a $200ms$ interval. To compute this quantity we set the JSR load to a fixed concentration $c_{jsr}$ at time $t = 0$ and then compute the number of times a Ca wave occurred within $200ms$ in 100 independent simulation runs. In Figure 5C we plot the probability of a wave occurring within a $200ms$ interval, denoted as $p_w$ (blue solid line), as a function of the initial $c_{jsr}$. As expected, we find a sharp sigmoid dependence of the wave nucleation probability as a function of the JSR load.

To explain our findings above, we first note that the transmission probability $p_{ij}$ determines the interaction between CRUs. Thus, we expect that the threshold of the wave nucleation probability should coincide with the threshold of $p_{ij}$. To confirm this hypothesis, we have computed the transmission probability $p_{ij}$ directly from simulations of the Restrepo cell model. To compute this probability we simply trigger a Ca spark at a specific CRU and compute

the fraction of times that a nearest neighbor site also fires within $20ms$. In this way we compute the JSR load dependence of the tranmission probability, which we denote as $p_{ij}^r$ (Figure 5C, red dashed line), directly from the 3D stochastic model. On the same graph we also plot our theoretical prediction for $p_{ij}$ using Eq. 10 (black dash-dotted line). Here, we find that the threshold for wave nucleation occurs at roughly the same range of concentrations as predicted by the transmission probability. However, the wave probability is substantially sharper, as a function of JSR load, than both the theoretical and numerically computed transmission probability.

To quantify the relationship between the wave threshold and the transmission probability we have computed these quantities for a range of cluster sizes $N$. In Figure 5D we plot the JSR load concentration $c_w$ such that $p_w(c_w) = 1/2$ (blue dash-dotted line). This quantity gives a measure of the onset of Ca wave nucleation as a function of system parameters. On the same graph we have also plotted the threshold of the transmission probability computed directly from the Restrepo model. This quantity is denoted as $\tilde{c}$ which satisfies $p_{ij}^r(\tilde{c}) = 1/2$ (red dashed line). Finally, we also show our theoretical prediction $c_{jsr}^*$ from Eq. (13) (black line). Indeed, we see that the onset of wave propagation coincides approximately with the threshold of the transmission probability. Thus, our results indicate that $c_{jsr}^*$ gives a quantitative approximation for the onset of Ca waves.

## IV. Nonlinear wave onset as a mechanism for alternans

The nonlinear relationship between the wave propagation probability and the JSR load will influence the dynamics of Ca cycling at the whole cell level. Here, we explore how this relation influences the beat-to-beat response of a cardiac cell when it is paced with a periodic AP clamp. As a starting point, we first analyze the response of the Ca cycling system to a single AP under varying initial JSR loads. In this case, the membrane depolarization during the AP upstroke induces LCC channels to open and trigger Ca sparks in the cell. The amount of Ca released during the AP clamp will be crucially dependent on two factors: (i) The onset of the JSR load dependence of the wave propagation probability $p_w$, which will dictate the conditions for waves to propagate. (ii) The fraction of clusters that are triggered by LCC channels, which determines the number of available RyR clusters, which can support Ca wave propagation. Note that the fraction of RyR clusters in the vicinity of LCC channels can vary between different cell types and under conditions of heart failure. To explore the role of these features we compute the peak diastolic Ca transient, denoted as $c_i^{max}$, in response to an AP and under a range of JSR loads. In Figure 6A we plot $c_i^{max}$ vs $c_{jsr}$ in the case where $30, 50, 70$ percent of the clusters have LCC channels. Indeed, we find that when most clusters are triggered by LCC channel openings then the presence of Ca waves plays little role in the response to an AP, since there are no available RyR clusters to sustain waves. However, when the density of LCC channels is reduced then $c_i^{max}$ exhibits a highly nonlinear response as a function of JSR load, since above the propagation transition Ca waves are induced and the amount of Ca release increases substantially.

Under periodic pacing conditions, the nonlinear response between Ca wave propagation and JSR load can drive Ca alternans. In Figure 6B, we plot the steady state JSR load as a function of time using a 3D cell model where only 30% of the dyadic junctions contain LCC channels. Indeed, we find that when the cell is paced at $T = 200ms$ then Ca release alternates from one-beat to the next. Simultaneous line scan imaging (Figure 6C) reveals that on the large beat Ca release is enhanced since LCC channel openings initiate Ca waves which propagate into the cell. Indeed, the JSR load clearly alternates above and below the threshold concentration for wave propagation (Figure 6B). To explore the rate dependence of alternans we have also computed the bifurcation diagram of the system. In Figure 7 we show the peak of the Ca transient for the last two beats after pacing for 20 beats at a cycle length $T$. In this case we simulate the condition where the fraction of release sites with LCC channels is 30% (black circles) and 50% (red squares). Indeed, we find that the system exhibits a typical period doubling bifurcation as the pacing cycle length is decreased. Furthermore, we observe that the onset of alternans shifts to smaller cycle lengths as the fraction of LCC channels is increased. This result is consistent with Figure 6A which shows that the amount of Ca released into the cell as a function of SR load becomes more steep as the density of LCC channels is reduced. Hence, the system is more prone to the alternans instability when the signaling fidelity between LCC and RyR clusters is reduced.

## Discussion

In this paper, we have shown that the onset of Ca waves is a sharp sigmoid function of the SR load. This result is consistent with experimental studies showing that Ca waves occur only at elevated SR loads, a feature referred to as store-overload-induced Ca release (SOICR) [31]. In particular, Jiang et al. [12] measured the occurrence of Ca waves in populations of cells and showed that the fraction of cells displaying waves exhibited a sigmoid relationship on the Ca content in the cell. Also Diaz et al. [32] measured the frequency of Ca waves in isolated myocytes and found that below a critical SR load Ca waves did not occur, but occurred with high frequency above that threshold. This result is consistent with several studies showing that the SR load dependence of Ca release exhibits a highly nonlinear threshold relationship[33]. In this study, we have identified the key features of the Ca signaling architecture that determines the onset and nonlinearity of this SR load dependence. Our main result is that the onset of Ca waves is dictated by the transmission probability $p_{ij}$, which is the probability that a Ca spark induces a nearest neighbor to fire. Using a master equation approach we have shown that the transmission probability is nonlinear function of SR load, since spark activation can be mapped to a barrier hopping process that is exponentially sensitive to system parameters. It is this exponential sensitivity which underlies the nonlinearity of signaling between RyR clusters, and consequently determines the onset of Ca waves in cardiac cells. Based on this result we have developed a quantitative estimate, given by Eq. 13, for the onset of Ca waves in cardiac myocytes. In particular, we point out the dependence of the onset on the parameter $\beta$, which is the ratio of the rise in local Ca concentration due to the diffusive flux from a nearest neighbor, to the SR load. This quantity is dependent on a variety of factors such as the distance between the clusters, the diffusion coefficient of Ca in the

intracellular space, and also the presence of Ca buffers. Hence, $\beta$ serves as a measure of the effective strength of the diffusion mediated coupling between RyR clusters in the cell. Also, the threshold depends on the parameter $\alpha$, which gives the ratio of the rise in local Ca concentration due to an RyR channel opening to the SR load. This quantity also depends on a variety of factors such as the volume of the dyadic junction, and the conductance of the RyR channel. Hence, our findings give a quantitative relationship between local signaling at the ion channel scale to arrhythmogenic whole cell events such as Ca waves.

The analysis in this paper reveals that the underlying nonlinearity can be traced to the architecture of Ca signaling in cardiac myocytes. In particular we identify two essential features leading to the nonlinear sigmoid dependence of the transmission probability: (i) An RyR channel has multiple Ca binding sites that regulate the transition from the closed to open state of the channel. This property is well known from experiments on isolated RyR channels which show that the open probability increases in a nonlinear fashion with the Ca concentration on the cytoplasmic side of the channel [34]. To incorporate this feature in our model we make the RyR closed to open rate proportional to the square of the local Ca concentration ($\gamma = 2$). (ii) RyR clusters have 50-150 channels that gate cooperatively due to the local diffusion of Ca. This feature has been established by super resolution imaging of subcellular Ca proteins in rat ventricular cells which reveal that the average channel number is roughly 60 channels [35,36]. Incorporating both of these features within our master equation approach revealed that the dynamics of an RyR cluster can be mapped to a nonlinear birth-death process. This process can be described by an effective potential which exhibits two local minima separated by a potential barrier, so that spark activation is equivalent to a barrier hopping process where the system transitions between these minima. A crucial requirement for this feature is that $\gamma \geq 2$, which indicates that Ca binding cooperativity underlies the main features of stochastic Ca signaling. The main consequence of this property is that all the statistical features of spark activation acquire an exponential dependence on system parameters that modulate the barrier height. Therefore, the observed nonlinear onset of Ca waves is a direct consequence of basic features of the Ca signaling architecture. In several studies it has been shown that RyR channels are sensitive to the Ca concentration in the SR [31,33]. In our analysis luminal gating can be described by allowing the RyR forward rate $k_+$ to depend on the JSR concentration. Indeed, Eq. 13 predicts that such a dependence will have a direct effect on the Ca wave onset. However, we point out that the sharp nonlinearity does not rely on luminal gating. Thus, luminal gating will serve to shift the onset of Ca waves but is not essential to explain the nonlinear behavior of Ca signaling.

Our findings reveal that the threshold for wave propagation is well predicted by $p_{ij}$, which is the transmission probability between clusters on the same Z-plane. However, this probability only dictates propagation within a Z-plane, and does not imply propagation between planes. This is because the cluster spacing within a Z-plane ($\sim 500nm$) is typically smaller than the spacing between adjacent Z-planes ($\sim 2\mu m$). Thus, it is necessary to compare $p_{ij}$ in both the transverse and longitudinal directions in the cell. Our simulations reveal that, for the

parameters of the Restrepo model, both of these distributions are similar. The reason for this is that in the Restrepo model the diffusion time constant in the longitudinal and transverse directions are similar. This choice of time constants are based on experimental observations which reveal that Ca waves are approximately spherical, which implies that longitudinal coupling between clusters should be roughly the same as that in the transverse direction [37]. This is likely due to a higher density of diffusional barriers in the transverse rather than longitudinal direction, which compensates for the distance anisotropy. This result explains why $p_{ij}$ between sites on the same Z-plane is sufficient to predict the Ca wave onset in the cell.

An important finding in this paper is that the probability of wave propagation $p_w$, shown in Figure 5C (solid blue line) is a sharp sigmoid function of the SR load. In particular we note that the wave threshold increases from $p_w \sim 0$ to $p_w \sim 1$ for a change of SR load of roughly $30\mu M$, which is substantially sharper than the SR load dependence of $p_{ij}$. Thus, while the transmission probability correctly predicts the onset of wave propagation it does not directly account for the sharpness of the nonlinear dependence. To explain this result we note that wave nucleation is likely due to spontaneous Ca sparks which induce a chain reaction of sparks, which can then summate to sustain a propagating wave front. Let us assume that a critical number of sparks, denoted as $n_c$, will have to fire in order to nucleate a propagating wave. The probability that a spontaneous spark in the cell leads to a chain reaction of $n_c$ sparks is then $\sim p_{ij}^{n_c}$. Therefore, the average waiting time for a wave can be approximated as $T_{wave} \sim T_s/p_{ij}^{n_c}$, where $T_s$ is the mean time between spontaneous Ca sparks. Thus, the cooperativity necessary to nucleate a wave amplifies the nonlinearity of $p_{ij}$ by the critical number of sparks $n_c$. However, the critical number of sparks $n_c$, which itself depends on the SR load, is not known and is likely difficult to determine analytically. Here, we emphasize our basic finding that cooperativity between clusters amplifies the intrinsic nonlinear signaling between clusters, so that the onset of Ca waves is substantially sharper than the local signaling nonlinearity.

In this study, we have also analyzed the beat-to-beat response of a spatially distributed Ca cycling model. Interestingly, we find that the nonlinear dependence of Ca wave onset on the SR load has a strong influence on the response of the system to periodic pacing. In particular, we showed that when the system is paced close to the Ca wave onset then the beat-to-beat response of the system displays Ca transient alternans. This finding is consistent with experimental and theoretical studies [19,21,22] showing that large amplitude alternans of the Ca transient during alternans correspond to a release sequence where Ca waves are observed on the large beat, but not on the small. This nonlinear response is due to the steep release load relationship that is observed near the wave onset transition. However, it should be noted that this nonlinearity is only exposed under specific conditions where the number of sparks recruited at pacing rates below the alternans transition is small. This condition applies in the case where a large fraction of release units lack LCC channels, so that only a small fraction of units fire in response to

an action potential. Under these conditions, a cell paced near the threshold for Ca waves will be unstable to Ca transient alternans. This mechanism is particularly relevant in heart failure where it is known that the close positioning between LCC and RyR clusters is disrupted[23]. In this case a large number of RyR clusters lack nearby LCCs so that the cell is more prone to propagating Ca waves, and is therefore more unstable to alternans. An important finding of this study is that these wave induced alternans are due to the nonlinear signaling between Ca release units. Thus, our theory of the nonlinear onset of Ca waves can be used to quantify the underlying mechanism for wave induced alternans. Here we also point out that alternans can also occur due to an alternative mechanism that is due to an order-disorder transition in large ensembles of Ca release units [25,38]. There, global alternans occurred when local all-or-none responses at Ca release units where synchronized by local Ca diffusion. In the mechanism presented here, the global response is due to a propagating Ca wave and not to the onset of synchronization which occurs at rapid rates. However, in both cases the underlying nonlinearity can be traced to local stochastic signaling that is due the architecture of Ca signaling in cardiac cells.

In this study, we have presented a quantitative theory of the nonlinear onset of Ca waves. These findings identify the important physiological parameters that set the threshold and degree of nonlinearity of the SR load dependence of Ca waves. Thus, these findings can serve as a guide in the development of therapeutic approaches, which target both Ca waves and alternans. In particular, our study highlights the importance of the quantity $\beta$ which is the ratio of the rise of local Ca concentration, due to diffusion from a nearest neighbor, to the JSR load. This quantity is dependent on a variety of factors such as the distance between RyR clusters, the diffusion of Ca in the intracellular space, and also the distribution and kinetics of buffers. Our analysis reveals that if $\beta$ is reduced then the threshold for Ca waves shifts to larger SR loads (Eq. 13). Thus, any mechanism that decreases $\beta$ will reduce the frequency of Ca waves and the degree of Ca transient alternans in the cell. Perhaps the most natural approach to control this parameter is by changing the concentration and distribution of Ca buffers in the cell. For example, buffers located in the subcellular volume between Z-planes will reduce the probability of plane-to-plane excitations and shift the onset of Ca waves to higher SR loads. However, it should be stated that a basic limitation of all proposals seeking to perturb the Ca cycling system is that these changes may disrupt Ca signaling processes, which are vital to other cellular process. Here, we point out that buffers offer a unique flexibility to control the rise in local Ca concentration since buffer kinetics can be tuned to act only at the elevated Ca levels that are relevant during Ca overload. In addition, immobile buffers can be targeted to specific sites in the cell where they will serve as diffusion barriers, while having a potentially minimal effect on the overall rise in Ca concentration in other parts of the cell. For instance, a major Ca buffer in the cell is Troponin C which is bound to actin myofilaments located between Z-planes. It may be worthwhile to explore the possibility of tuning the binding affinity of Troponin C to Ca in order to suppress large Ca fluxes which induce activation between Z-planes. In this way it may be possible to reduce dynamical instabilities by controlling the rate of Ca diffusion between different parts of the cell. Thus,

our approach, by uncovering the essential mechanism for the nonlinearity underlying Ca wave onset and alternans, suggests novel antiarrhythmic strategies, which have yet to be explored.


## Acknowledgement

This work was supported by the National Heart, Lung, and Blood Institute grant RO1HL101196.


**Table 1.** Model parameters modified from the original Restrepo computational cell model.

| Parameter | Description | Value |
|---|---|---|
| $\tau_i^T$ | Transverse cytosolic diffusion time | $1.47ms$ |
| $\tau_i^L$ | Longitudinal cytosolic diffusion time | $1.16ms$ |
| $\tau_s^T$ | Transverse submembrane diffusion time | $0.71ms$ |
| $\tau_s^L$ | Longitudinal submembrane diffusion time | $0.85ms$ |
| $\tau_{NSR}^T$ | Transverse NSR diffusion time | $3.60ms$ |
| $\tau_{NSR}^L$ | Longitudinal NSR diffusion time | $12.0ms$ |
| $K_u$ | CSQN-unbound opening rate | $1.5 \times 10^{-4}(\mu M)^{-2}ms^{-1}$ |
| $N$ | Number of channels in RyR cluster | 100 |

**Table 2**. Parameters used to compute effective potential.

| Parameter | Description | Value |
|---|---|---|
| $k_+$ | RyR opening rate | $1.5 \times 10^{-4}(\mu M)^{-2}ms^{-1}$ |
| $k_-$ | RyR closing rate | $1.0\ (ms)^{-1}$ |
| $\gamma$ | Exponent of Ca binding | 2 |
| $N$ | Number of channels in cluster | 100 |
| $\tau_s$ | Spark lifetime | $15ms$ |
| $\beta$ | Ratio of the peak Ca concentration due to the diffusive flux from a neighboring spark to the JSR load. | $2.5/1000$ |
| $\alpha$ | Ratio of the dyadic junction concentration due to one open RyR channel to the JSR load. | $5.0/1000$ |
| $s_{on}$ | Dimensionless parameter during nearest neighbor | 0.5 |

| | | |
|---|---|---|
| | spark. | |
| $s_{off}$ | Dimensionless parameter in the absence of a nearest neighbor spark. | 0.04 |

## Figure Captions

**Figure 1**. (A) Schematic illustration of the spatial architecture of Ca signaling in a cardiac ventricular cell. Signaling between channels occur within dyadic junctions distributed in the 3D volume of the cell. (B) Illustration of two nearest neighbor signaling units (CRUs) showing the subcellular compartments. Here, the superscript $n$ denotes the $n^{th}$ CRU in a 3D grid representing the cell. (C) Spatial architecture of the cell interior showing Z-planes.

**Figure 2.** (A) The local Ca concentration $c_p^i$ at junction $i$ in which a Ca spark occurs. In this simulation a spark is induced in that junction by raising the local concentration above the threshold for spark activation. Here, the initial JSR load is $c_{jsr} = 1000\mu M$, and the Ca concentration rises to a peak of roughly $c_p \sim 300\ \mu M$. (B) The local concentration $c_p^j$ at a nearest neighbor junction $j$ on the same Z-plane. Here, the local flux due to the RyR cluster is set to zero so that the rise in concentration is due only to the diffusive flux from junction $i$. At this site the local concentration rises to $\sim 3\mu M$.

**Figure 3.** (A) The effective potential $\Phi(x)$ for spark off (black solid line, $s_{off} = 0.04$), and spark on (red dashed line, $s_{on} = 0.5$). As $s$ is increased the barrier height between the stable stationary point at $x_o$ and the unstable point at $x_1$ is reduced. (B) Plot of the stationary points $x_o$ and $x_1$ as a function of the parameter $s$.

**Figure 4.** (A) The effective potential barrier $N\Delta\Phi$ as a function of the JSR load $c_{jsr}$ for the spark on case $s = 0.5$. (B) The waiting time vs the JSR load computed using an exact stochastic simulation of an isolated cluster of $N = 100$ RyR channels. (C) The transmission probability $p_{ij}$ as a function of the JSR load computed using the exact stochastic simulation (red dashed line) and from Eq. (10) (black solid line). (D) The threshold for transmission probability $c_{th}$ is computed as the JSR load where $p_{ij}(c_{th}) = 1/2$, where $p_{ij}$ is computed with the exact stochastic simulation (black circles). $c_{jsr}^*$ (red squares) is computed using our analytic approximation given by Eq. (13).

**Figure 5.** Ca wave nucleation and propagation in a 3D stochastic cell model. (A) Spatial distribution of dyadic junction Ca concentration $c_p^n$ visualized across a 2D cross section of a cell with $20 \times 20 \times 60$ CRUs. (B) The mean waiting time $T_w$ for a Ca wave as a function of JSR load. Points shown are averaged over 100 independent simulations. (C) The probability $p_w$ of a Ca wave occuring within a $200ms$ time interval as a function of the JSR load (blue solid line). Line is computed by averaging over 100 independent simulations. The transmission probability between two adjacent units, denoted as $p_{ij}^r$, computed using the Restrepo model (Red dashed line).

The transmision probability computed using Eq. 10 (black dash-dotted line). (D) The threshold as a function of the number of channels in the cluster $N$. Blue dash-dotted line corresponds to the wave propagation onset $c_w$ defined as $p_w(c_w) = 1/2$. Red dashed line is the SR load such that $p_{ij}^r(\tilde{c}) = 1/2$ computed directly from the Restrepo model, and black solid line is the analytic threshold given by Eq. 13.

**Figure 6.** (A) The calculated peak of diastolic Ca concentration, $c_i^{max}$, as a function of $c_{jsr}$ for cases where 30% (black, bottom line), 50% (red, middle line), and 70% (top, blue line), percent of the clusters have LCC channels. (B) Time dependence of the steady state JSR load simulated using a 3D cell model where only 30% of the clusters are driven by LCC channels. In this case the cell is paced with an AP clamp with a period of $T = 200\,ms$. The shape of the AP clamp is the same as that used in the original Restrepo model. (C) Simulated line scan of subcellular Ca release during alternans.

**Figure 7.** Plot of the peak Ca transient $c_i^{\max}$ for the last 2 beats after pacing the cell for 20 beats. Black circles and red squares correspond to 30% and 50% LCC density respectively.

## References


[1] M. D. Bootman and M. J. Berridge, Cell **83**, 675 (1995).
[2] H. Cheng and W. J. Lederer, Physiol Rev **88**, 1491 (2008).
[3] D. M. Bers, Nature **415**, 198 (2002).
[4] D. M. Bers, *Excitation-contraction coupling and cardiac contractile force* (Kluwer Academic Publishers, Dordrecht ; Boston, 2001), 2nd edn., Developments in cardiovascular medicine, 237.
[5] L. T. Izu, W. G. Wier, and C. W. Balke, Biophysical journal **80**, 103 (2001).
[6] B. D. Stuyvers, P. A. Boyden, and H. E. ter Keurs, Circulation research **86**, 1016 (2000).
[7] G. Hernandez-Hernandez, E. Alvarez-Lacalle, and Y. Shiferaw, Physical review. E, Statistical, nonlinear, and soft matter physics **92**, 052715 (2015).
[8] T. Takamatsu and W. G. Wier, Faseb J **4**, 1519 (1990).
[9] H. E. Ter Keurs and P. A. Boyden, Physiol Rev **87**, 457 (2007).
[10] Z. Song, C. Y. Ko, M. Nivala, J. N. Weiss, and Z. Qu, Biophysical journal **108**, 1908 (2015).
[11] Y. Xie, D. Sato, A. Garfinkel, Z. Qu, and J. N. Weiss, Biophysical journal **99**, 1408 (2010).
[12] D. Jiang, R. Wang, B. Xiao, H. Kong, D. J. Hunt, P. Choi, L. Zhang, and S. R. Chen, Circulation research **97**, 1173 (2005).
[13] V. Lukyanenko and S. Gyorke, The Journal of physiology **521 Pt 3**, 575 (1999).
[14] M. Nivala, C. Y. Ko, M. Nivala, J. N. Weiss, and Z. Qu, Biophysical journal **102**, 2433 (2012).
[15] M. Nivala, C. Y. Ko, M. Nivala, J. N. Weiss, and Z. Qu, The Journal of physiology **591**, 5305 (2013).
[16] Y. Shiferaw, M. A. Watanabe, A. Garfinkel, J. N. Weiss, and A. Karma, Biophysical journal **85**, 3666 (2003).

[17] S. M. Pogwizd and D. M. Bers, Trends Cardiovasc Med **14**, 61 (2004).
[18] Z. Qu, M. Nivala, and J. N. Weiss, Journal of molecular and cellular cardiology **58**, 100 (2013).
[19] M. E. Diaz, S. C. O'Neill, and D. A. Eisner, Circulation research **94**, 650 (2004).
[20] J. Huser, Y. G. Wang, K. A. Sheehan, F. Cifuentes, S. L. Lipsius, and L. A. Blatter, The Journal of physiology **524 Pt 3**, 795 (2000).
[21] T. Tao, S. C. O'Neill, M. E. Diaz, Y. T. Li, D. A. Eisner, and H. Zhang, American journal of physiology. Heart and circulatory physiology **295**, H598 (2008).
[22] Q. Li, S. C. O'Neill, T. Tao, Y. Li, D. Eisner, and H. Zhang, Biophysical journal **102**, 1471 (2012).
[23] M. Nivala, Z. Song, J. N. Weiss, and Z. Qu, Journal of molecular and cellular cardiology **79**, 32 (2015).
[24] J. G. Restrepo, J. N. Weiss, and A. Karma, Biophysical journal **95**, 3767 (2008).
[25] J. G. Restrepo and A. Karma, Chaos **19**, 037115 (2009).
[26] G. A. Langer and A. Peskoff, Circulation **96**, 3761 (1997).
[27] M. Asfaw, E. Alvarez-Lacalle, and Y. Shiferaw, PloS one **8**, e62967 (2013).
[28] R. Hinch, Biophysical journal **86**, 1293 (2004).
[29] C. Doering, K. Sargsyan, and L. Sander, SIAM Journal of Multiscale Modeling & Simulations **3**, 283 (2005).
[30] K. S. Charles Doering, Leonard Sander, Eric Vanden-Eijnden, J. Phys. :Condens. Matter **19**, 065145 (2007).
[31] W. Chen *et al.*, Nature medicine **20**, 184 (2014).
[32] M. E. Diaz, A. W. Trafford, S. C. O'Neill, and D. A. Eisner, The Journal of physiology **501 ( Pt 1)**, 3 (1997).
[33] T. R. Shannon, K. S. Ginsburg, and D. M. Bers, Biophysical journal **78**, 334 (2000).
[34] M. Fill and J. A. Copello, Physiol Rev **82**, 893 (2002).
[35] Y. Hou, I. Jayasinghe, D. J. Crossman, D. Baddeley, and C. Soeller, Journal of molecular and cellular cardiology **80**, 45 (2015).
[36] D. Baddeley, I. D. Jayasinghe, L. Lam, S. Rossberger, M. B. Cannell, and C. Soeller, Proceedings of the National Academy of Sciences of the United States of America **106**, 22275 (2009).
[37] J. Engel, M. Fechner, A. J. Sowerby, S. A. Finch, and A. Stier, Biophysical journal **66**, 1756 (1994).
[38] E. Alvarez-Lacalle, B. Echebarria, J. Spalding, and Y. Shiferaw, Physical review letters **114**, 108101 (2015).

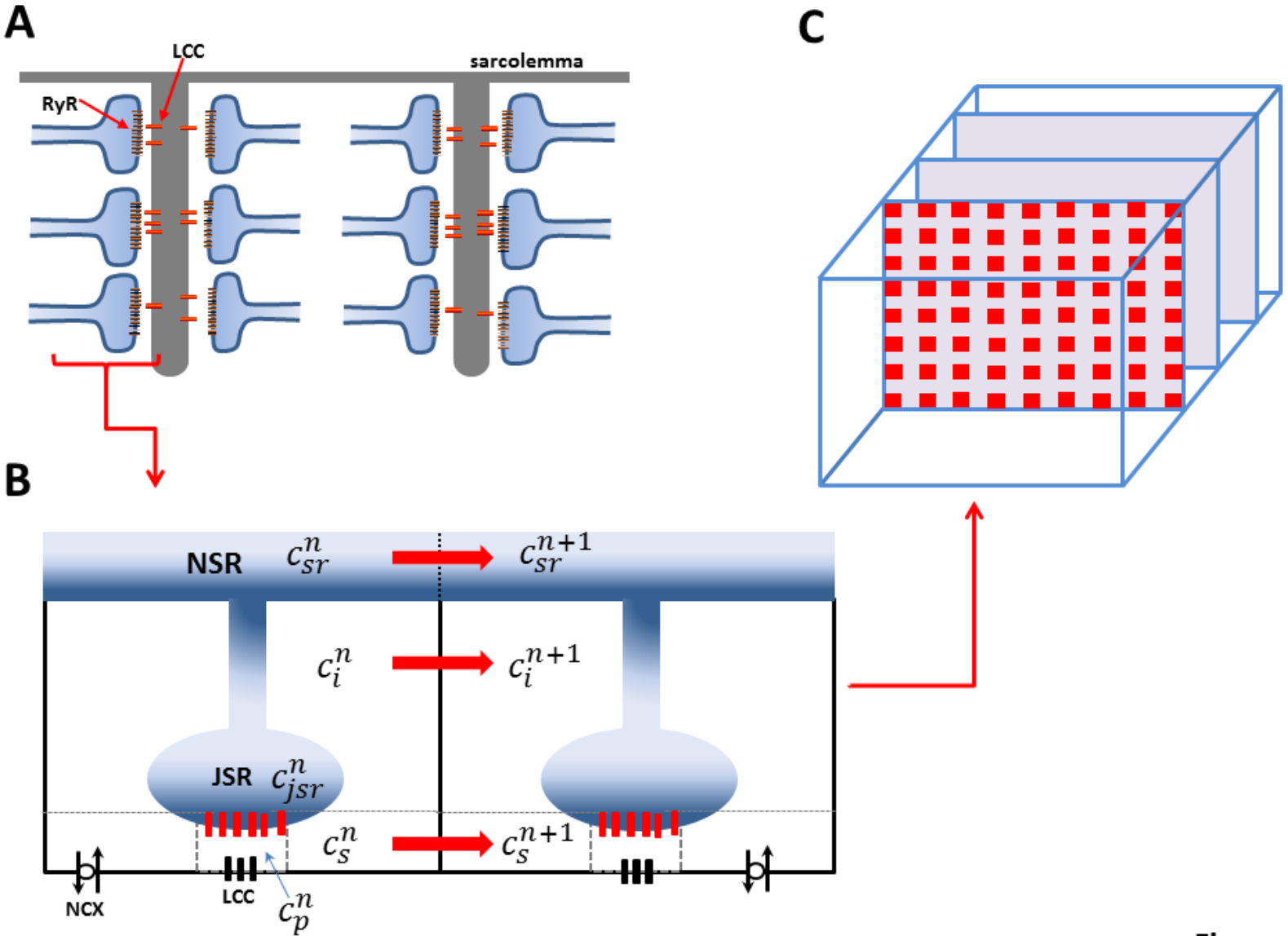
A
LCC
sarcolemma
RyR
C
B
NSR
$c_{sr}^n$
$c_{sr}^{n+1}$
$c_i^n$
$c_i^{n+1}$
JSR
$c_{jsr}^n$
$c_s^n$
$c_s^{n+1}$
NCX
LCC
$c_p^n$

Figure 1

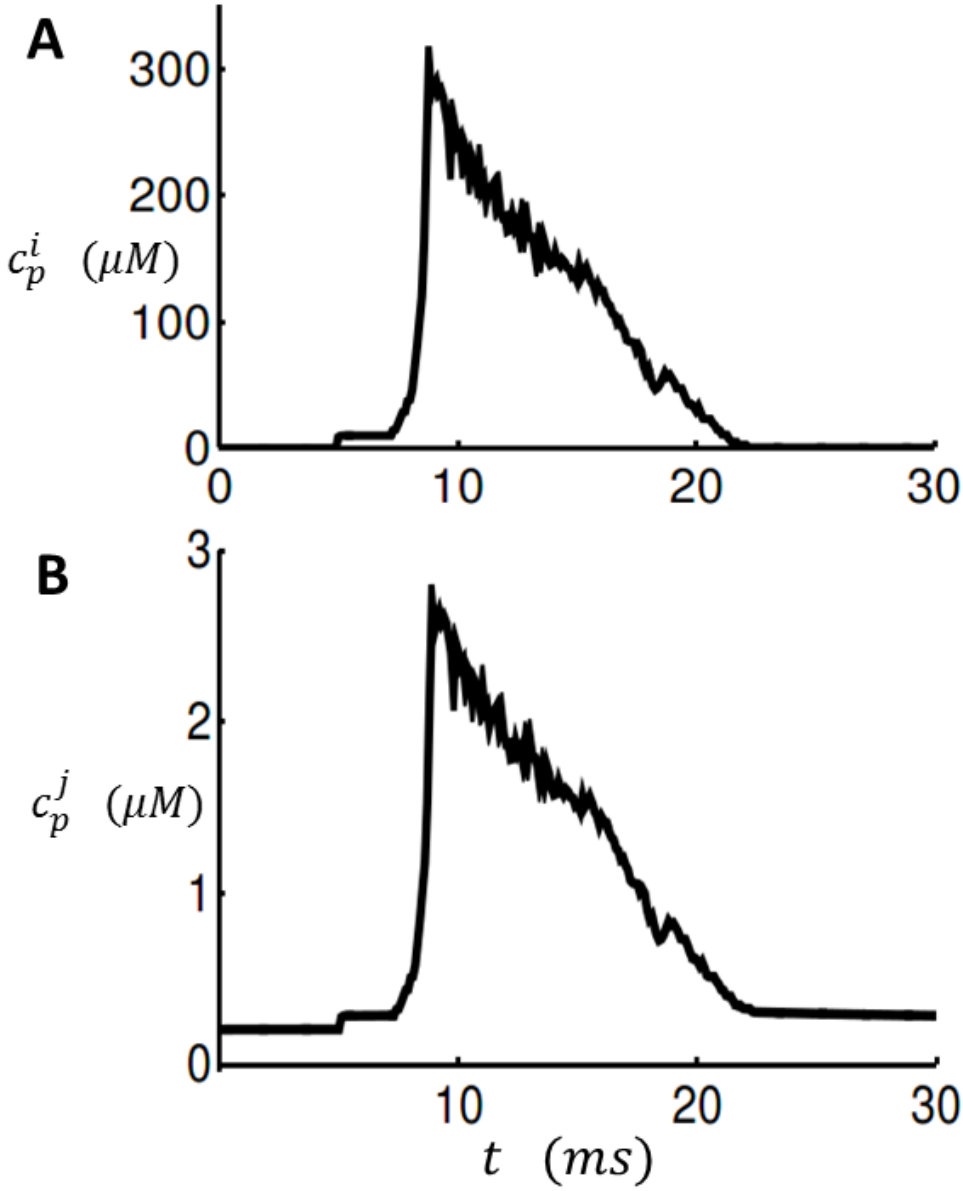


Figure 2

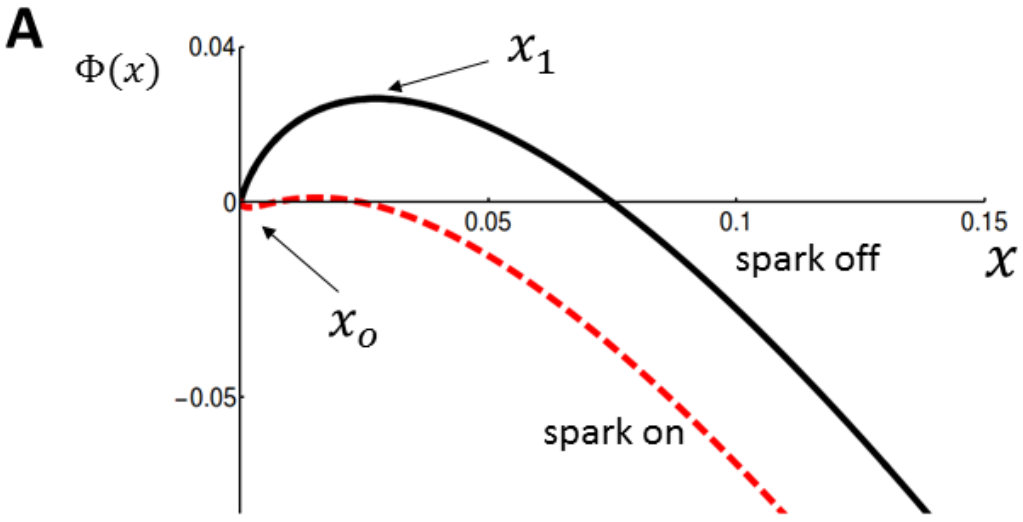
A
$\Phi(x)$
0.04
0
−0.05
$x_1$
$x_o$
0.05
0.1
0.15
spark off
spark on
$x$

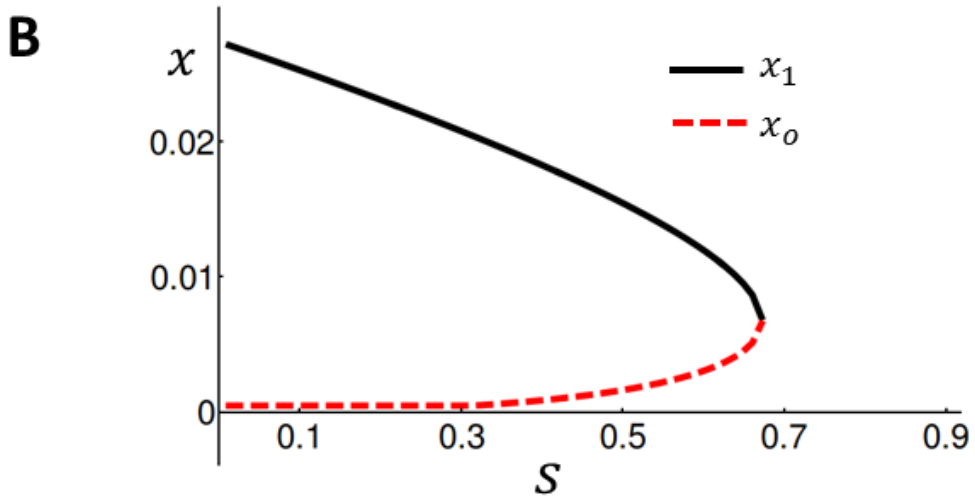
B
$x$
0.02
0.01
0
$x_1$
$x_o$
0.1
0.3
0.5
0.7
0.9
$S$

**Figure 3**

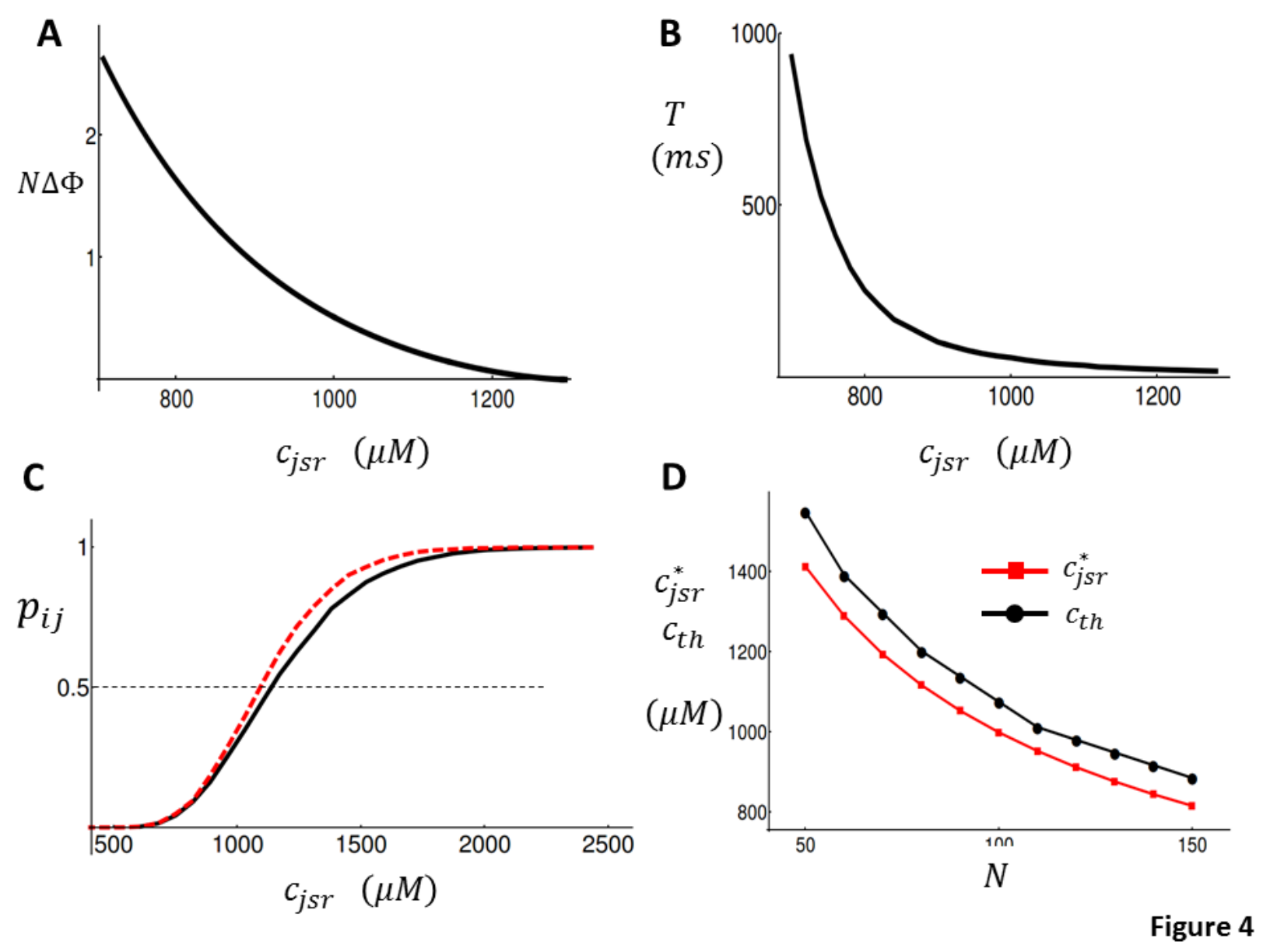
A
$N\Delta\Phi$
2
1
800
1000
1200
$c_{jsr}$ $(\mu M)$
B
$T$
$(ms)$
1000
500
800
1000
1200
$c_{jsr}$ $(\mu M)$
C
$p_{ij}$
1
0.5
500
1000
1500
2000
2500
$c_{jsr}$ $(\mu M)$
D
$c^*_{jsr}$
$c_{th}$
$(\mu M)$
1400
1200
1000
800
50
150
$N$
$c^*_{jsr}$
$c_{th}$

**Figure 4**

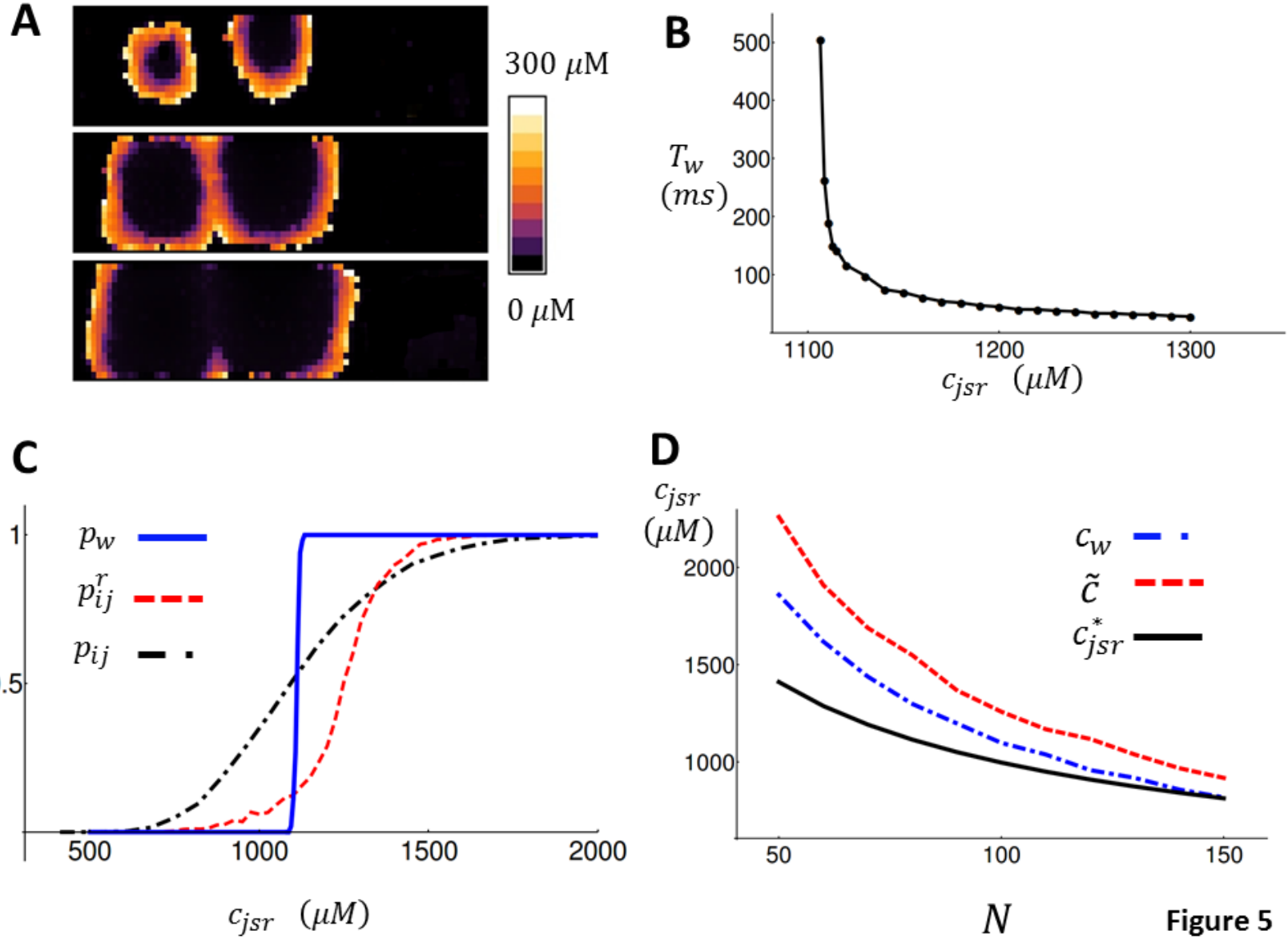
A
300 $\mu$M
0 $\mu$M
B
$T_w$ $(ms)$
500
400
300
200
100
1100
1200
1300
$c_{jsr}$ $(\mu M)$
C
$p_w$
$p_{ij}^r$
$p_{ij}$
1
0.5
500
1000
1500
2000
$c_{jsr}$ $(\mu M)$
D
$c_{jsr}$ $(\mu M)$
2000
1500
1000
$c_w$
$\tilde{c}$
$c_{jsr}^*$
50
100
150
$N$

**Figure 5**

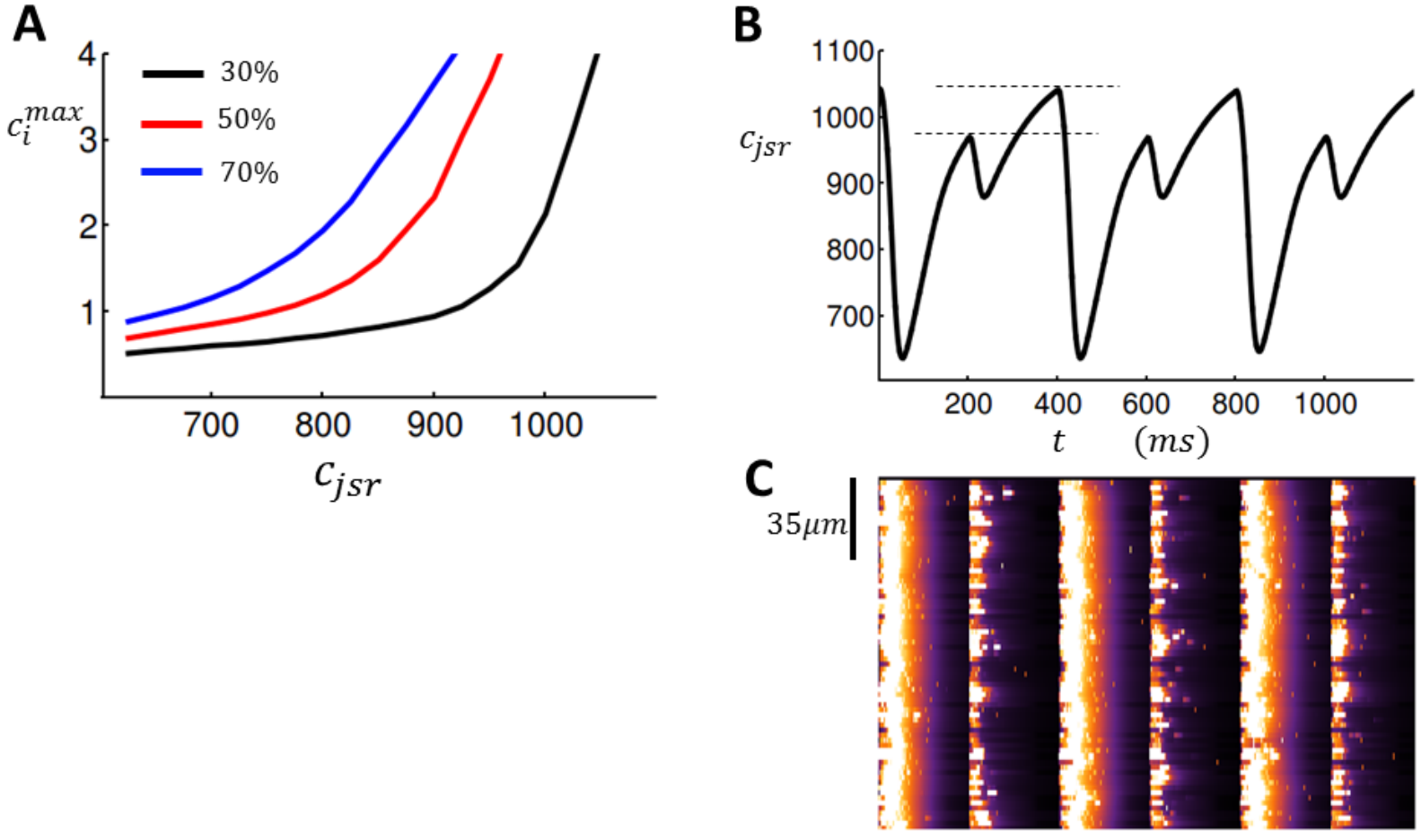
A
$c_i^{max}$
4
3
2
1
30%
50%
70%
700
800
900
1000
$c_{jsr}$
B
1100
1000
900
800
700
$c_{jsr}$
200
400
600
800
1000
$t$ $(ms)$
C
$35\mu m$

Figure 6

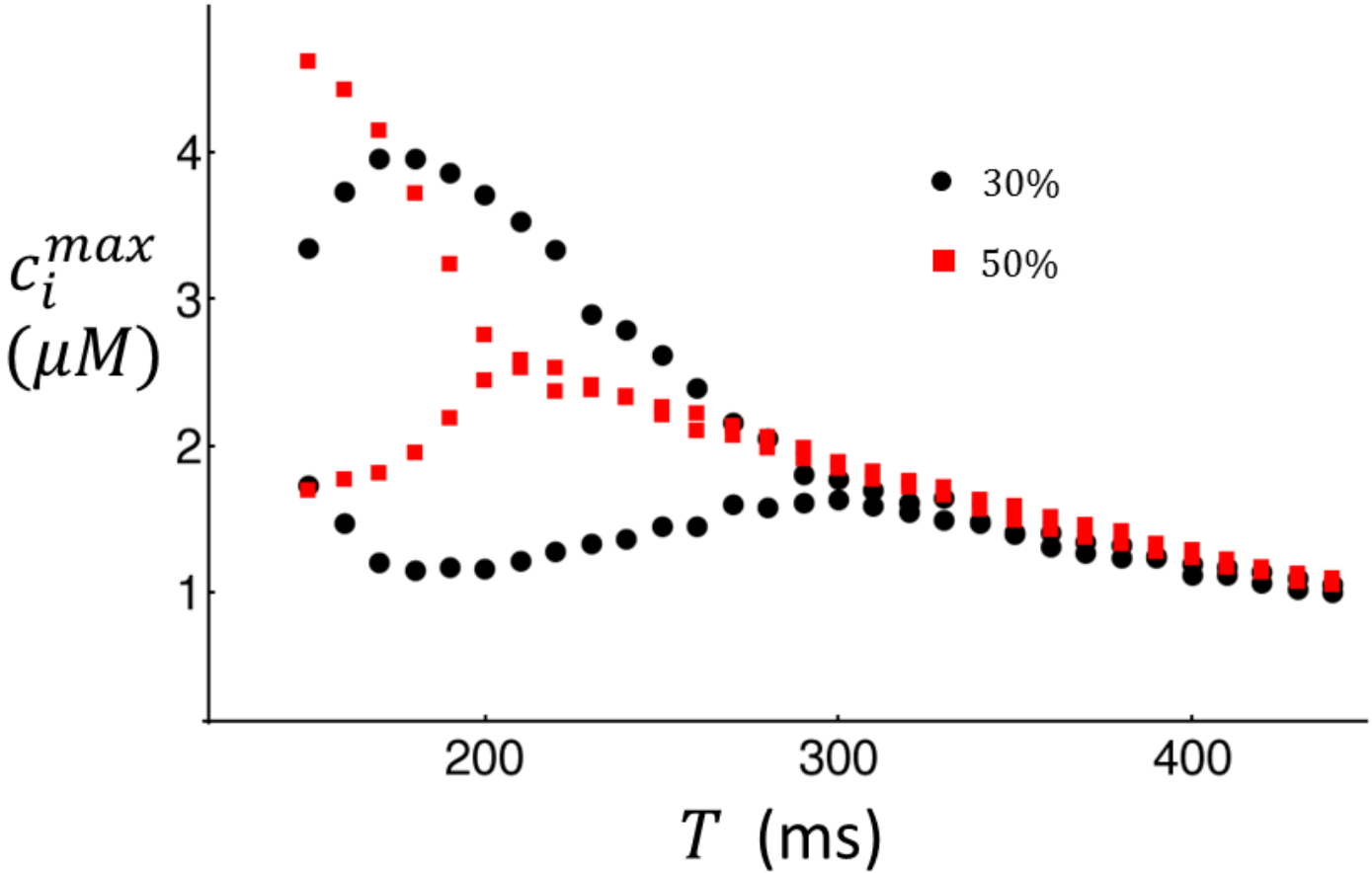


Figure 7